Table 1 Derived wind velocity from secular decrease in inclination

1) Satellite	2) Average perigee height, km	3) $(\Delta i)_1$	4) $(\Delta i)_2$	5) $(\Delta i)_{theo}$	6) $(\Delta i)_{obs}$	7) Residuals	8) Wind velocity (implied), mph
1958 Alpha	355	−0°.0152	−0°.0152	−0°.0152	−0°.0208	−0°.0056 ± 25	368 ± 164
1958 Gamma	188	−0°.0452	−0°.0454	−0°.0453	−0°.0524	−0°.0071 ± 42	157 ± 93
1958 Delta 2	221	−0°.0448	−0°.0453	−0°.0451	−0°.0535	−0°.0084 ± 34	186 ± 75

tions, separated by more than 400 days. The inclinations used here are plotted, along with their standard errors, in Fig. 3. The least-squares expression for the inclination is

$$I = (65°.1629 \pm 03) - (0°.1277 \pm 82) \times 10^{-3} [t\text{-December 7, 1958}] \pm 0°.0003 \text{ (S.D.)}$$

Results

Table 1 gives the values of the secular decrease in the inclinations of the three satellites. Column 3 shows the theoretical decrease in inclination derived by using Eq. (1), and column 4 shows the same decrease obtained through Eq. (2). Column 5 gives the mean of columns 3 and 4. Column 6 gives the observed secular decrease computed from least-squares expressions for inclination. Column 7 lists the residuals, along with their standard deviations.

These results are more accurate than others so far published. For each one of the three satellites, the author clearly has a higher secular decrease in the inclination than that predicted on the assumption of the solid-body rotation of the atmosphere, which conforms to the results of other authors. Column 8 of Table 1 gives the velocity of the wind, necessary to explain the higher observed secular decrease in the inclination of the three satellites. The results appear to suggest winds moving at high speeds in the upper atmosphere. If winds moving at speeds high enough to explain the higher

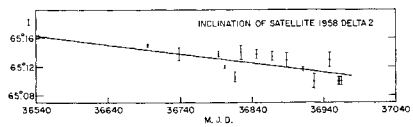

Fig. 3 The solid line shows the least-squares linear expression for inclination against the observed values with their standard deviations

secular decrease in inclination seem unlikely, one should obviously look for some other phenomenon that might account for the increased transverse acceleration on the motion of the artificial satellites.

References

[1] Merson, R. H. and King-Hele, D. G., "Use of artificial satellites to explore the earth's gravitational field: Results from Sputnik 2 (1957 β)," Nature **182**, 640–641 (1958).

[2] Wildhack, W. A., "Effect of transverse atmospheric drag on satellite orbits," Science **128**, 309–310 (1958).

[3] Sterne, T. E., "Effect of the rotation of a planetary atmosphere upon the orbit of a close satellite," ARS J. **29**, 777–782 (1959).

[4] Cornford, E. C., "A comparison of orbital theory with observations made in the United Kingdom on the Russian satellites," Royal Aircraft Establishment (July 1958).

[5] Bosanquet, C. H., "Change of inclination of a satellite orbit," Nature **182**, 1533 (1958).

[6] Plimmer, R. N. A., "The effect of the earth's atmospheric rotation on the orbital inclination of a near-earth satellite," Royal Aircraft Establishment TN 504 (1959).

[7] Cook, G. E. and Plimmer, R. N. A., "The effect of atmospheric rotation on the orbital plane of a near-earth satellite," Proc. Roy. Soc. (London) **A258**, 516 (1960).

[8] Cook, G. E., "Effect of an oblate rotating atmosphere on the orientation of a satellite orbit," Proc. Roy. Soc. (London) **A261**, 246–258 (1961).

[9] Vinti, J. P., "Theory of the effect of drag on the orbital inclination of an earth satellite," J. Res. Natl. Bur. Std. **62**, 79–88 (1959).

Graphical Method for Optimization of Cesium-Surface Ionizer Materials

G. Kuskevics*
Electro-Optical Systems, Inc., Pasadena, Calif.

A graphical method is proposed for the optimization of cesium ionizer material, structure, and operating point. Proper selection of the ionizer material, its structure and work function, and the design point would optimize the propellant-utilization efficiency, power efficiency, and, to some extent, life of the cesium-ion engine. The method is illustrated 1) by optimization of the design point for a solid tungsten ionizer using exponential and linearized plots and 2) by selection of optimum material based on preliminary experimental critical temperature T_c curves and theoretical neutral fraction α curves.

1. Introduction

THE performance of a surface-ionization cesium ionizer is determined by ionization efficiency, ion-generation energy efficiency, and lifetime. The ionization efficiency β is defined as the ratio of the ion efflux to the total cesium efflux. The ion-generation energy efficiency η is the ratio of the ionization potential to the ion-generation energy. These ionizer figures of merit directly determine the propellant-utilization efficiency and the overall ion-engine power efficiency, respectively. Historically, ionizers and their design points have been selected to give very high (near unity) ionization efficiency regardless of the ion-generation energy efficiency. The best overall performance is obtained if these two opposing figures of merit are simultaneously optimized. The ionizer lifetime sets an upper limit of operating temperature. Similarly, limits are set by breakdown voltage on the ion-current density and by electrode life on the ionization efficiency.

2. Graphical Optimization of the Ionizer Design Point

A graphical method for selection of the optimum design-operating point for a given ionizer is illustrated by its application to a solid tungsten ionizer. The ionization efficiency β vs T_c and the specific ion-generation energy, p/j vs T_c plots are superimposed in Fig. 1. The β curve is a plot of the Saha-Langmuir equation for a constant work function

Received by ARS July 29, 1962; revision received April 15, 1963.

* Senior Scientist, Ion Physics Department. Member AIAA.

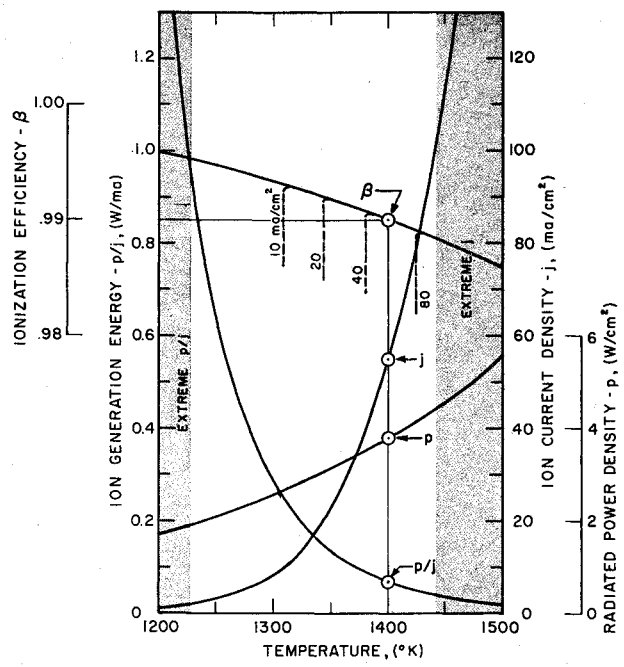

Fig. 1 Nonlinearized graphs for the optimization of the ionizer design point using solid tungsten as an example

of 4.52 ev. The p/j curve gives the energy required to generate an ion in w/ma or kev/ion. p/j varies as the inverse of the ion-generation energy efficiency. For completeness the curves for p vs T_c and j vs T_c are given also. The lower temperature limit is set by the extreme power requirement, the upper limit by electrical breakdown of the very small gaps because of the high voltage required to overcome the space charge at very high current densities. The β and p/j curves in Fig. 1 show how much ionization efficiency is sacrificed by going to a higher ion-generation efficiency (lower p/j). A lower limit on the ionization efficiency may be set by engine electrode life. The electrode erosion for accurately designed accelerator geometry is caused mostly by the interception of ions from charge exchange. This charge exchange occurs when beam ions hit slow neutral atoms producing a fast neutral atom and a slow ion. Low ionization efficiency increases the density of the slow neutral atoms and the ions produced by charge exchange. If a lower limit of $\beta = 0.99$ is set by charge exchange, then the optimum design point for solid W

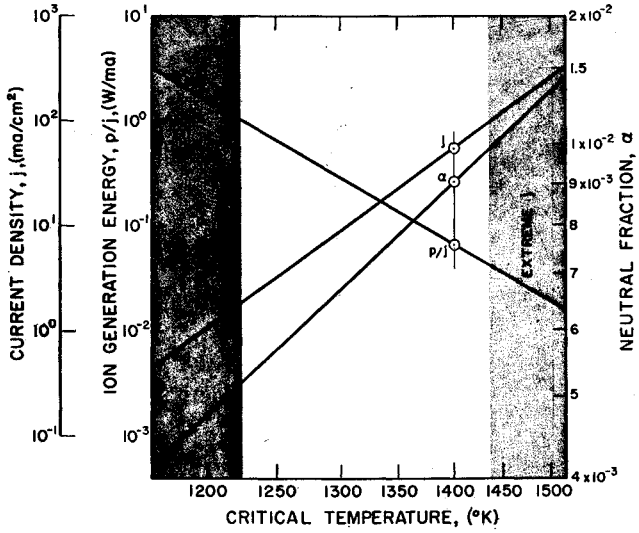

Fig. 2 Linearized graphs for the optimization of solid tungsten ionizer design point

is at 1400°K which gives the simultaneous values of $\beta = 0.99$, $j = 55$ ma/cm², and $p/j = 0.7$ w/ma.

For easier plotting and data extrapolation the graphs can be linearized. The ionization efficiency β can be replaced by the neutral fraction α. $\beta = 1/(1 + \alpha) \approx 1 - \alpha$ for $\alpha \ll 1$. Much higher experimental accuracy is achieved by the measurement of the neutral fraction instead of the ionization efficiency. The $\log_{10} \alpha$, $\log_{10} (p/j)$, and $\log_{10} j$ vs $1/T_c$ plots are given in Fig. 2. The graphs are represented by the following equations.

$$\beta = \frac{1}{1 + 2 \exp\,(-e\Delta E)/kT]}$$

$$\log j = 11.993 - 14350/T_c \text{ (ma/cm}^2\text{)}$$

$$p = 5.67 \times 10^{-12}\, \epsilon T^4 \text{ (w/cm}^2\text{)}$$

$$\frac{p}{j} = \frac{5.67 \times 10^{-12}\, \epsilon T^4}{10^{11.993 - 14350/T}} \text{ (w/ma)}$$

The case of solid tungsten just treated represents a very idealized case for which the data are well known. However,

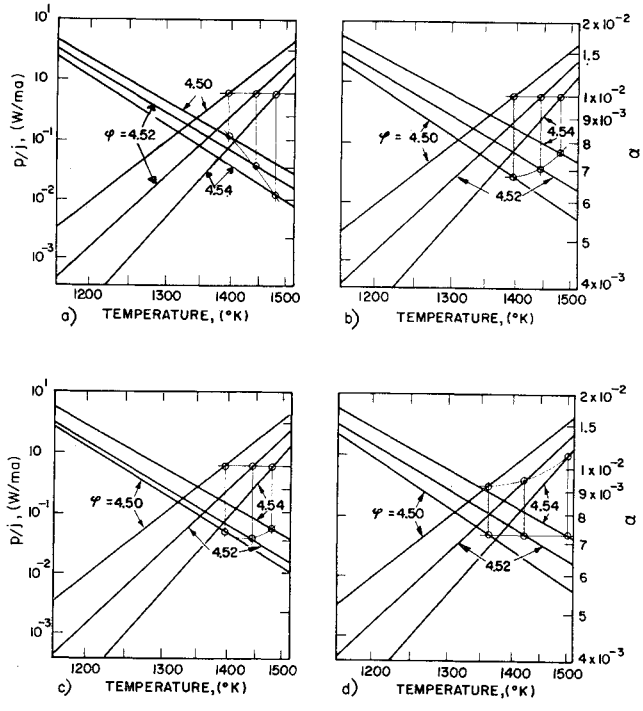

Fig. 3 Possible trends in the optimization of ionizer work function

the graphical method is applicable to any experimental data even if they cannot be represented by similar equations. The linearized plot should be used even if the graphs become somewhat nonlinear.

3. Optimization of Ionizer Work Function

The work function of solid or porous tungsten is known to depend upon preferential crystal orientation (by thermal etching, e.g.), upon doping (thoriated tungsten), or upon adsorbed layers of gas (such as oxygen). Tungsten ionizers with continuous oxygenation are used in mass-spectrometer ion sources to ionize alkali earth metals. Some of the oxide impurity dissolved in the cesium is decomposed and the oxygen is chemisorbed on the ionizer. The addition of a controlled amount of oxygen to the cesium or continuous oxygenation from a separate supply of oxygen can be used to control the work function of the ionizer. Ionizers of similar design are expected to have a statistical distribution of average work functions.

Assuming that the work function of the ionizer can be either selected or changed in a controllable manner, the graphical method can be used for the optimization of its value to achieve the best performance. Figure 3 shows three sets of graphs illustrating three possible trends. Experimental α and p/j curves are plotted for three values of average work function φ. The graphs for $\varphi = 4.52$ ev are the same as those for solid tungsten. Assume that the maximum allowable $\alpha = 0.01$. The p/j graphs for different ionizers may follow an increasing trend as shown in Fig. 3a. For this case the optimum work function is the highest φ leading also to high operating temperatures and high ion-current densities. If the trend of p/j graphs is as shown in Fig. 3b, then the reverse is true. For the same trend, but a nonlinear spacing as in Fig. 3c, there exists a minimum p/j that is not due to upper limits of β or j. Figure 3d illustrates the selection of work function for a given ion generation efficiency p/j. For the p/j graph trend the minimum α is obtained with the minimum φ.

Since the radiated power density depends upon the emittance of the ionizer which can vary without regard to the

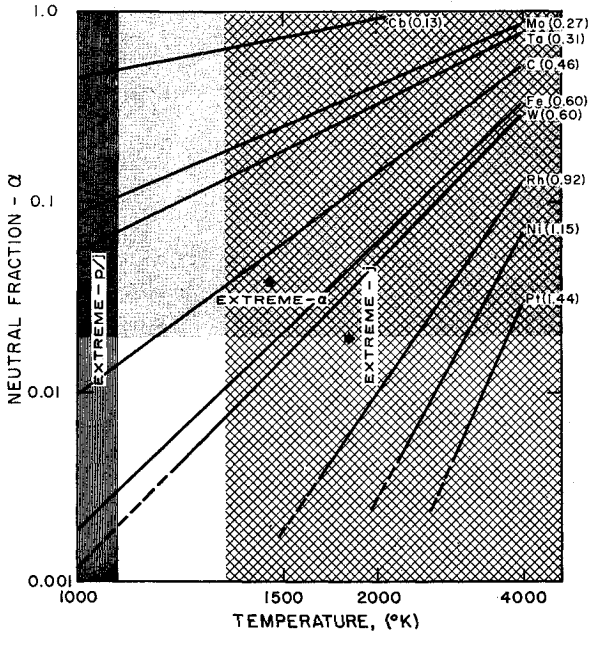

Fig. 4 Selection of materials within the limits of various ionizer parameters. Numbers in parentheses are values of ΔE in electron volts

average work function, the p/j trend could be either as in Fig. 3a or in Fig. 3b.

4. Selection of Optimum Ionizer Material

Different refractory metals that satisfy the secondary requirements of high melting point and low vapor pressure, in general, have high work functions ranging from 4 to 5.5 ev. Selection of tungsten for the ionizer material was due to the abundance of experimental data which demonstrated very low neutral fraction and the availability and advanced technology for making porous structures. The ion-generation energy requirement was not considered. If a strict upper limit of 0.02 is placed on the value of α, materials such as Cb, Mo, and Ta could be eliminated unless their work functions are higher than the preferred values used in Fig. 4. If the upper limit of ion-current density due to electrical breakdown and perveance limitations is 100 ma/cm^2, the upper limit of operating temperature is at about 1450°K. This temperature limit applies only to tungsten. The temperature limit corresponding to 100 ma/cm^2 would be different for the other materials, however, it is expected to eliminate work functions corresponding to preferred average values for Rh, Ni, Re, and Pt. The actual measured work functions of the materials vary over a considerable range. Therefore, the simple theory limits the values of $\Delta E = \varphi - V_i$ to a range of 0.45 to 0.9 ev ($\varphi = 4.33$ to 4.78 ev). For the actual selection of porous ionizer materials, experimental values of α should be used.

The graphical method of cesium ionizer optimization is applied to preliminary experimental data[1] of j vs T_c. Neither the power loss due to thermal radiation nor the emittance was measured. However, the method of comparison can be illustrated by making the assumption that the emittances are equal and independent of T. From the experimental j vs T_c graphs one can obtain T^4/j graphs that represent the relative P/j in Fig. 5. The theoretical neutral fractions are

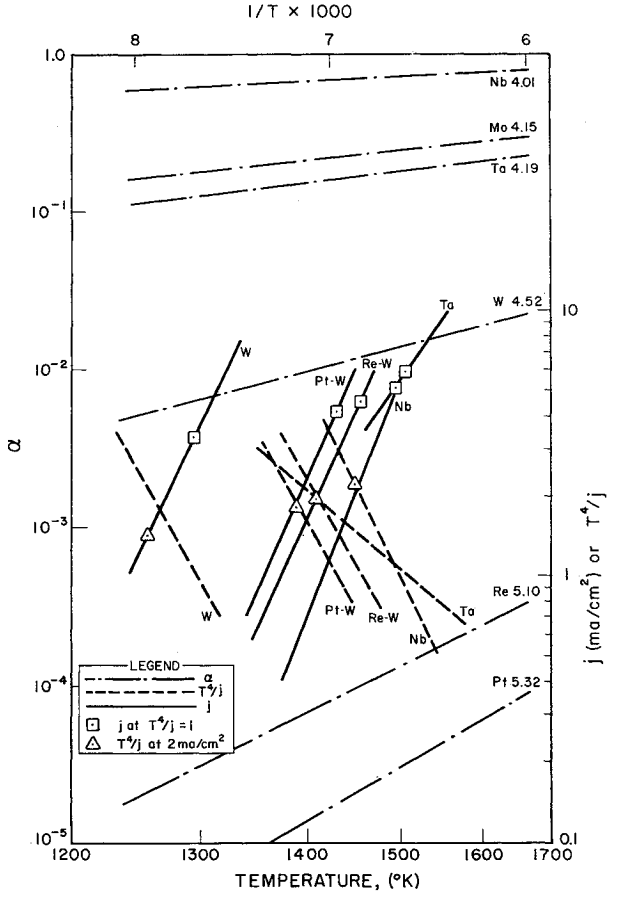

Fig. 5 Construction for the optimization of cesium ionizer materials using preliminary experimental data

shown for completeness, even though the values of α are not within the desired limits just discussed.

Experimental neutral-fraction data must be used for the material selection. A limited comparison is possible on the basis of the T^4/j graphs in Fig. 5. The lowest value of T^4/j at $j = 2$ ma/cm^2 can be attained with a W ionizer and it increases with Pt-W, Re-W, Ta, and Nb. There is some doubt about the correctness of data for Ta and Nb because of their high permeability and the large difference in the slope for Ta curves. A similar order, except for Ta, is observed for a constant T^4/j. A more detailed description of this method is available.[2]

References

[1] Kuskevics, G., Worlock, R. M., and Zuccaro, D., "Ionization, emission and collision processes in the cesium ion engine,"

Progress in Astronautics and Rocketry: Electric Propulsion Development, edited by E. Stuhlinger (Academic Press Inc., New York, 1962), Vol. 9, pp. 229–268.

[2] Kuskevics, G., "Criteria and a graphical method for optimization of cesium surface ionizer materials," Electro-Optical Systems Research Rept. 3 (January 1962).

Axially Loaded Column Subjected to Lateral Pressure

JAMES P. PETERSON*
NASA Langley Research Center, Hampton, Va.

THE buckling behavior of columns subjected to axial load and lateral pressure is of general interest in aerospace applications and in the industrial manufacture of extrusions. A solution to this problem may be derived rather easily and, surprisingly, it is not generally known. Consider the column shown in the sketch at the top of Fig. 1; it is subjected to an end load pA and a lateral pressure q. The cross-sectional shape of the column is shown circular but it may be any shape that is constant with the coordinate x including closed thin-wall tubular shapes. The coordinate z is taken normal

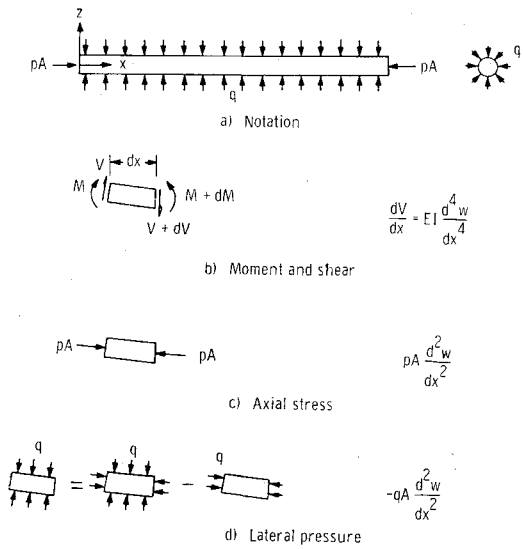

Fig. 1 Lateral forces entering into the equilibrium of an element of a buckled column

to the axis of the least moment of inertia of the cross section of the column.

A differential equation for the lateral deflection w of the column may be obtained from considerations of the equilibrium of an element of the buckled column. For equilibrium in the direction of z, the following equation is obtained as the sum of the terms listed on the right-hand side of Fig. 1b–1d.

$$EI\ (d^4w/dx^4) + (p - q)A(d^2w/dx^2) = 0 \qquad (1)$$

The qA term (Fig. 1d) is obtained without the necessity of integrating over the surface of the column element by making use of the fact that any body subjected to hydrostatic pressure is in equilibrium.

Received March 15, 1963.

* Head, Structural Strength Section. Member AIAA.

Solution of Eq. (1) leads to the eigenvalue

$$(p - q) = p_0 \qquad (2)$$

or to

$$(p/p_0) - (q/p_0) = 1 \qquad (3)$$

where p_0A, which is a function of the boundary conditions at the ends of the column, is the compressive axial load required to buckle the column in the absence of lateral pressure, and A is the cross-sectional area of solid-section columns and is the area enclosed by the outside dimensions of the walls of tubular columns. Equation (3), which gives the interaction between axial and lateral pressure on column buckling and which is independent of boundary conditions, is plotted in Fig. 2. It can be seen from Fig. 2 that a column in a hydrostatic pressure field lies in the stable region and requires an additional end load equal to p_0A in order to reach the stability boundary; the hydrostatic pressure may be a tensile or negative pressure and, in the case of a closed tubular strut, may be produced by internal pressure. Hence a tubular strut subjected to tensile stresses of pressurization and to a compressive axial load equal to the column buckling load of the unpressurized tube will buckle even though the tensile stresses of pressurization may be greater than the compressive stresses from the axial load; that is, it is possible for a tube to buckle as a column while subjected to tensile stresses in both the circumferential and axial directions. The pressures p and q of Eq. (3) and Fig. 2 are pressures applied to the outside of the column. Hence, for tubular columns where the area A enclosed by the outside dimensions of the tube differs

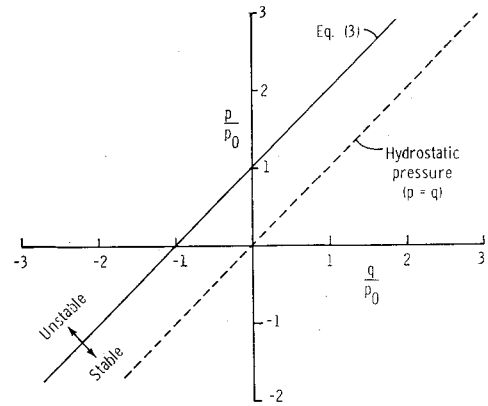

Fig. 2 Interaction curve for column subjected to axial load and lateral pressure

appreciably from the area A_i enclosed by the inside dimensions of the tube and where a hydrostatic pressure field is achieved by internal pressurization, a correction of A_i/A must be applied to the internal pressure in order to obtain the equivalent external pressure required in Eq. (3) and Fig. 2.

Solutions to the stability of pressurized circular thin-wall columns subjected to the particular loading case $p = 0$ and $q = -p_0$ are given in Refs. 1 and 2. The stability of rectangular solid sections is discussed in Ref. 3, but erroneous conclusions are drawn because of an incorrect sign on the pressure q in the equation of Ref. 3 corresponding to Eq. (2) of the present note.

References

[1] Nagel, F. E., "Column instability of pressurized tubes," J. Aerospace Sci. **23**, 608–609 (1956).

[2] Mills, B. D., Jr., "The fluid column," Am. J. Phys. **28**, 353–356 (1960).

[3] Kerr, A. D., "On the instability of elastic solids," Proc. Fourth U.S. Natl. Congr. Appl. Mech. **1**, 647–656 (1962).